

# DETERMINISTIC SIZE EFFECT IN CONCRETE SIMULATED WITH TWO VISCOPLASTIC MODELS

ANDRZEJ WINNICKI<sup>1</sup>, ADAM WOSATKO<sup>2</sup> AND MICHAŁ SZCZECINA<sup>3</sup>

<sup>1</sup> Faculty of Civil Engineering, Cracow University of Technology  
Warszawska 24, 31-155, Cracow, Poland  
andrzej@hypatia.L5.pk.edu.pl, www.wil.pk.edu.pl

<sup>2</sup> Faculty of Civil Engineering, Cracow University of Technology  
Warszawska 24, 31-155, Cracow, Poland  
awosatko@L5.pk.edu.pl, www.wil.pk.edu.pl

<sup>3</sup> Faculty of Civil Engineering and Architecture, Kielce University of Technology  
Tysiąclecia Państwa Polskiego Ave. 7, 25-314, Kielce, Poland  
michalsz@tu.kielce.pl, www.wbia.tu.kielce.pl

**Key words:** Concrete, Size effect, Viscoplasticity, FEM

**Abstract.** The paper examines the ability of two selected viscoplastic models to reproduce the deterministic size effect in plain concrete specimens. The first one is the concrete damaged plasticity model and it is available in the ABAQUS package. The second one is the Hoffman viscoplastic consistency model and it is programmed in FEAP. Rate dependency existing in both models serves as a localization limiter leading to mesh-objective results for reasonably high values of viscosity, so the reproducing of the deterministic size effect is expected. Numerical analysis is performed for notched and unnotched beams under three point bending using both models. Additionally, the results are compared with the experiment made by Grégoire et al.

## 1 INTRODUCTION

The origin of the knowledge concerning the size effect in brittle and quasi-brittle materials can be traced back to the works of Galileo. Nowadays the subject has matured and usually a distinction is made between deterministic and stochastic size effects. In brittle and quasi-brittle materials deterministic size effect is more important than the stochastic one originating from the randomness of material strength [1]. There is extensive experimental evidence of the deterministic size effect in concrete, e.g. [2, 3]. Since the development of fracture mechanics the knowledge of size effect laws has also matured [4].

The ability of the both non-local integral or gradient (either in plastic or damage format) models to recreate the size effect in numerical simulations for concrete is well known and documented [5, 6]. Much less research has been done for viscoplastic models. Such models, similar to non-local or gradient models, can act as localization limiters and overcome in an effective way the spurious mesh dependency appearing in numerical solution for elements made of plain

concrete [7]. However, knowledge concerning their ability to reproduce the deterministic size effect is limited.

The aim of the paper is a numerical examination of the deterministic size effect in three-point bending for specimens made of plain concrete using two viscoplastic models. The first one is the Concrete Damage Plasticity (CDP) model with optionally included viscous term. The second one is the Hoffman viscoplastic consistency (HVP) model for concrete implemented in FEAP code [8] by authors. In the paper a new modified version of this model is presented assuming a non-associated flow rule with the plastic potential of the Drucker-Prager type. The numerical results are compared with the experiments reported in [9]. Two types of concrete beam specimens are analyzed – notched and unnotched.

## 2 REVIEW OF APPLIED MODELS

### 2.1 Concrete damaged plasticity model

The first model which is applied in computations was originally proposed in [10] and next enhanced in [11]. This model is distributed by ABAQUS software and called therein "damaged plasticity model for concrete and other quasi-brittle materials" [12], but here acronym CDP will be used. The theory of the plastic flow is non-associated in the CDP model. An application of viscous term and isotropic damage as additional components of the model is also possible.

The yield function is introduced in the stress space:

$$F_{\text{CDP}}^{\text{p}} = \frac{q + 3\alpha p + \beta(\tilde{\epsilon}^{\text{p}}) \langle \sigma_{\text{max}} \rangle - \gamma \langle -\sigma_{\text{max}} \rangle}{1 - \alpha} - \sigma_c(\tilde{\epsilon}_c^{\text{p}}) = 0 \quad (1)$$

where  $p = -\frac{1}{3}\sigma_{ii}$  is the hydrostatic pressure and  $q = \sqrt{\frac{3}{2}s_{ij}s_{ij}}$  is the Mises deviatoric measure of stress tensor  $\sigma$ . The parameter  $\alpha$  depends on the relation of the uniaxial compressive strength  $f'_c$  to the biaxial compressive strength  $f'_{bc}$ . Function  $\beta(\tilde{\epsilon}^{\text{p}})$  changes according to stress-strain relationships defined separately for compression and for tension. The parameter  $\gamma$  decides about the shape of the yield surface in the deviatoric plane. The subscript  $\text{max}$  refers to the maximum principal stress, so  $\langle \sigma_{\text{max}} \rangle = \frac{1}{2}(\sigma_{\text{max}} + |\sigma_{\text{max}}|)$ . The example of the initial yield surface described in the plane stress state is depicted in Fig. 1(a). The uniaxial compressive strength  $f'_c$  and the uniaxial tensile strength  $f'_t$  and relation  $f'_{bc} = 1.16f'_c$  are according to the numerical analysis presented in this paper, see Table 2 and Fig. 4. Plastic potential in the CDP model flow is defined as follows:

$$G_{\text{CDP}}^{\text{p}} = [(e f'_t \tan \psi)^2 + q^2]^{1/2} + \tan \psi p \quad (2)$$

where  $e$  is the eccentricity of the plastic potential flow and  $\psi$  is dilatancy angle. This function is illustrated in Fig. 1(b) in the  $p - q$  plane for the exemplary data:  $e = 0.1$  (that value is default in ABAQUS for CDP),  $f'_t = 3.88$  MPa and  $\psi = 15^\circ$ .

In this paper the CDP model is equipped with a viscoplastic regularization according to the Duvaut-Lions approach [13] for the viscoplastic strain rate  $\dot{\epsilon}^{\text{vp}}$ :

$$\dot{\epsilon}^{\text{vp}} = (\epsilon^{\text{p}} - \epsilon^{\text{vp}}) / \mu \quad (3)$$

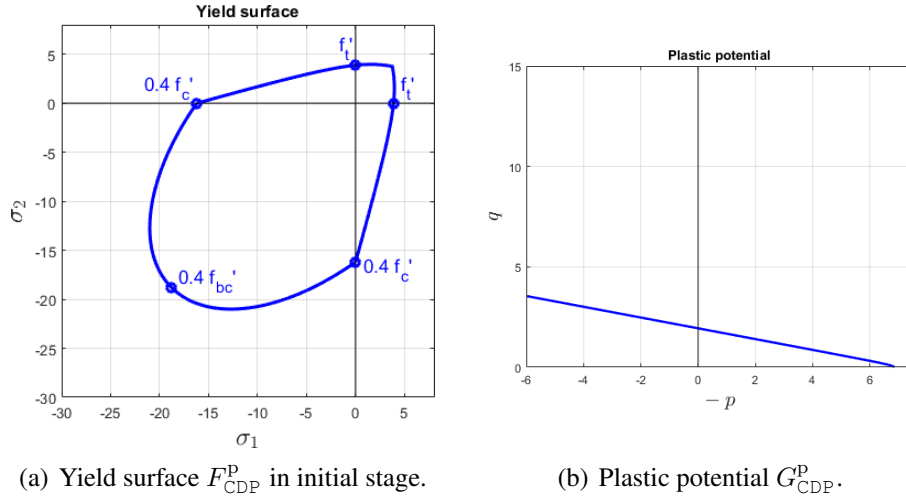


**Figure 1:** Exemplary yield and plastic potential functions for CDP model.

The viscous term for plastic strain  $\epsilon^{\text{P}}$  activates if only the relaxation time parameter  $\mu$  is larger than zero. The theory of plasticity described above can be combined with isotropic damage, but this coupling is not employed in the computations presented in the paper.

## 2.2 Hoffman viscoplastic consistency model

Usually the viscoplastic models follow the approaches proposed by Perzyna [14] or Duvaut-Lions [13] in which the viscoplastic strains are defined in explicit way using the viscosity parameter (relaxation time). A quite different approach was proposed by Wang [15] and called the consistency viscoplasticity. In the consistency viscoplasticity the yield function can expand or shrink depending on the actual viscoplastic strain rate. The stress state is forced to remain on the yield surface and the consistency condition is invoked. There is no need for an additional equation defining a viscoplastic multiplier. Instead, in the consistency condition two separate generalized material moduli appear: a classical plastic one  $h$  and a viscoplastic one  $s$ .

The Hoffman viscoplastic consistency (HVP) model for concrete uses the Burzyński-Hoffman yield surface in its isotropic form which has been successfully employed in the analysis of concrete structures [16]:

$$F^{\text{VP}} = q^2 - 3p(f_c - f_t) - f_c f_t = 0 \quad (4)$$

The yield surface (at the beginning of plastic processes) is presented in Fig. 2 (the plane stress state and  $p - q$  plane) for the data given in Table 2.

It is assumed that two internal variables  $\kappa_c$  and  $\kappa_t$  exist which are both functions of the equivalent viscoplastic strain. They describe in a separate way hardening/softening behaviour in compression and tension, respectively. In addition, two more internal variables  $\eta_c$  and  $\eta_t$  determine the increase/decrease of compressive and tensile strengths due to the actual rate of the equivalent viscoplastic strain. Thus, the actual compressive and tensile strengths are:

$$f_c = f_c(\kappa_c, \eta_c) \quad \text{and} \quad f_t = f_t(\kappa_t, \eta_t) \quad (5)$$

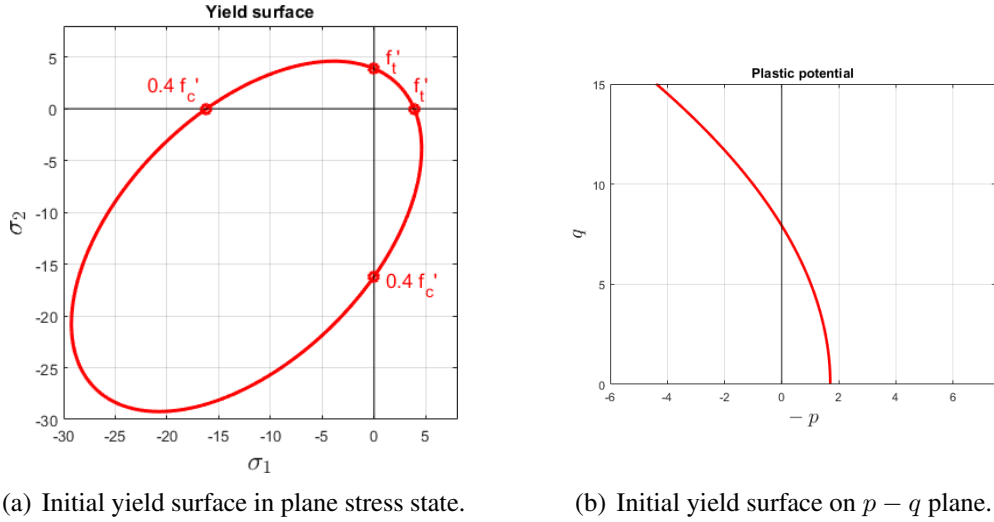


**Figure 2:** Exemplary yield function  $F^{\text{VP}}$  for HVP model.

The rates of the internal variables depend on the current stress and the rates of internal variables  $\kappa$  and  $\eta$ :

$$\dot{\kappa}_c = g_c(\boldsymbol{\sigma})\dot{\kappa} \quad \text{and} \quad \dot{\kappa}_t = g_t(\boldsymbol{\sigma})\dot{\kappa} \quad (6)$$

$$\dot{\eta}_c = g_c(\boldsymbol{\sigma})\dot{\eta} \quad \text{and} \quad \dot{\eta}_t = g_t(\boldsymbol{\sigma})\dot{\eta} \quad (7)$$

In the above equations  $g_c$  and  $g_t$  are scalar functions of stress accounting for independent processes of damage in compression and tension.

In turn,  $\dot{\kappa}$  is defined as an equivalent viscoplastic strain (in the rate form) assuming work hardening, and in a similar way  $\dot{\eta}$  depends on the first derivative of the viscoplastic strain (i.e. its rate is a function of the second derivative):

$$\dot{\kappa} = (\boldsymbol{\sigma} : \dot{\boldsymbol{\epsilon}}^{\text{VP}}) / q \quad \text{and} \quad \dot{\eta} = (\boldsymbol{\sigma} : \ddot{\boldsymbol{\epsilon}}^{\text{VP}}) / q \quad (8)$$

The dependence of  $f_c$  on  $\kappa_c$  and  $\eta_c$  is formulated in a general way as:

$$f_c = f'_c H_c(\kappa_c) S_c(\eta_c) \quad (9)$$

where  $f'_c$  is the initial compressive strength. Similarly, the actual tensile strength is:

$$f_t = f'_t H_t(\kappa_t) S_t(\eta_t) \quad (10)$$

Specific forms of these functions used in this paper are presented in Fig. 5.

The strain rate is decomposed into its elastic and viscoplastic parts:

$$\dot{\boldsymbol{\epsilon}} = \dot{\boldsymbol{\epsilon}}^e + \dot{\boldsymbol{\epsilon}}^{\text{VP}} \quad (11)$$

and the generalized Hooke's law is valid for the elastic part:

$$\dot{\boldsymbol{\sigma}} = \mathbf{D} : \dot{\boldsymbol{\epsilon}}^e \quad (12)$$

The viscoplastic flow is defined similarly to the classical rate independent plasticity using a notion of the plastic potential:

$$\dot{\epsilon}^{\text{vp}} = \dot{\lambda} \mathbf{m} \quad \text{where} \quad \mathbf{m} = \frac{\partial G^{\text{vp}}}{\partial \boldsymbol{\sigma}} \quad (13)$$

In the original version of the consistency model for concrete [17] the associated flow rule was assumed:

$$G^{\text{vp}} \equiv F^{\text{vp}} \quad (14)$$

There is an ample evidence that for concrete (at least for larger values of the hydrostatic pressure  $p$ ) that the associated flow rule leads to excessive plastic dilatancy – much larger than encountered in experiments [18]. As a remedy, the plastic potential in a form of the Prager-Drucker surface is proposed, where  $\psi$  is the dilatancy angle:

$$G^{\text{vp}} = q + \tan \psi p \quad (15)$$

At this stage of the development the examples presented in this paper, however, are computed using the original version of the model in its associated form.

In order to establish the viscoplastic multiplier  $\dot{\lambda}$  the consistency equation is used, which in its final form reads:

$$\dot{F}^{\text{vp}} = \mathbf{n} : \dot{\boldsymbol{\sigma}} - h \dot{\lambda} - s \ddot{\lambda} = 0 \quad (16)$$

where  $\mathbf{n} = \partial F^{\text{vp}} / \partial \boldsymbol{\sigma}$ ,  $h$  is the classical generalized plastic modulus and  $s$  is the generalized viscoplastic modulus. Due to the last term the consistency equation is no longer an algebraic equation for the viscoplastic multiplier, but a differential equation of the first order, to be solved for an appropriate initial condition. In the case when the functions  $S_c$  and  $S_t$  are constant, their derivatives vanish and Eq. (16) reduces to the form known from the classical rate independent plasticity.

### 3 BEAM UNDER THREE POINT BENDING – NUMERICAL STUDY

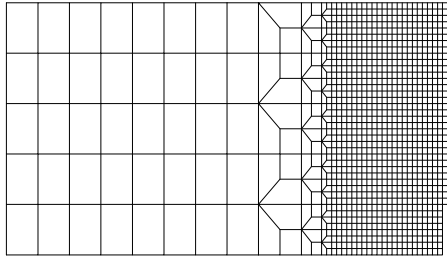
#### 3.1 Geometry and material model data

In the paper the size effect for viscoplastic models is verified for the beam test under three point bending. The geometry and material data as well as comparison with experimental results are taken from [9]. Two options are considered, i.e. the beam with and without the notch. The dimensions for all specimens are given in Table 1. Numerical simulations are performed for a half of the domain due to the symmetry, see Fig. 3. The mesh density is consistent with the sizes of the configuration, so the magnitude of finite elements changes proportionally to the geometry of specimens. Plane stress is assumed. Thickness  $t = 50$  mm is constant for all simulations. Displacement control is employed in numerical analyses. Four-noded elements with full integration are used as in the simulations in [9].

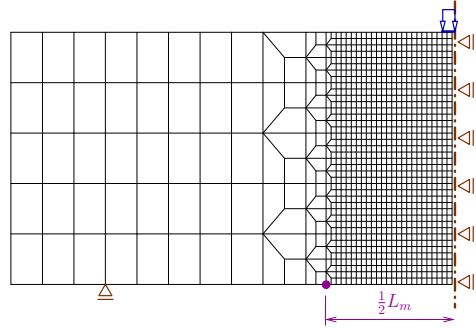
The material data for both models are listed in Table 2. In each model stress–strain relations for tension and compression are defined separately. The postcracking function for tension in the CDP model is determined as linear softening. It starts with strength  $f'_t = 3.88$  MPa and goes to residual strength  $0.01 f'_t$  for ultimate strain  $\epsilon_{tu}^{\text{cr}} = 0.002$ . Stress–inelastic strain function for

**Table 1:** Beam test – geometry.

Specimen	Length $L$ [mm]	Total height $D$ [mm]	Ligament height $D_{\text{lig}}$ [mm]	Span $S$ [mm]	Measurement base $L_m$ [mm]
DN1	1400	400	320	1000	400
DN2	700	200	160	500	200
DN3	350	100	80	250	100
DN4	175	50	40	125	50
DU1	1400	400		1000	400
DU2	700	200		500	200
DU3	350	100		250	100
DU4	175	50		125	50



(a) FE mesh for symmetric half of notched beam (N).



(b) Symmetric half of unnotched beam (U) with FE mesh.

**Figure 3:** Beam test under three point bending.

**Table 2:** Beam test – material model parameters.

Young's modulus:	$E = 37000 \text{ MPa}$	Tensile strength:	$f'_t = 3.88 \text{ MPa}$
Poisson's ratio:	$\nu = 0.21$	Compressive strength:	$f'_c = 42.3 \text{ MPa}$
<b>CONCRETE DAMAGED PLASTICITY (CDP)</b>		<b>HOFFMAN VISCOPLASTICITY (HVP)</b>	
Relation for compression:	Fig. 4	Material function $H_c$ :	Fig. 5(a)
Postcracking for tension:	linear softening	Material function $H_t$ :	Fig. 5(b)
Ultimate tensile strain:	$\epsilon_{tu}^{cr} = 2.0 \times 10^{-3}$	Material function $S_c = S_t$ :	Fig. 5(c)
Viscosity parameter:	$\mu = 2.0 \times 10^{-4} \text{ s}$	Work hardening	Eq. (8)
Dilatancy angle:	$\psi = 15^\circ$		

compression is shown in Fig. 4. Dilatancy angle  $\psi$  equals  $15^\circ$ . It is assumed that viscous term is activated in this model via parameter  $\mu = 0.0002 \text{ s}$ . The other model parameters are defaults, according to [12]. If the HVP model is taken into account, functions  $H_c(\kappa_c)$  for compression and  $H_t(\kappa_t)$  for tension are also defined in different ways, cf. Figs 5(a) and 5(b). However, functions of the equivalent viscoplastic strain rate, i.e.  $S_c(\eta_c)$  for compression and  $S_t(\eta_t)$  for tension, remain the same in these two regimes, see Fig. 5(c).

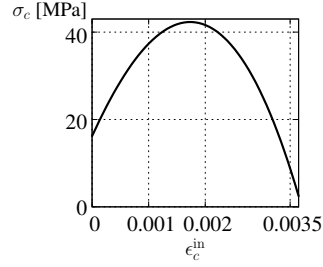


**Figure 4:** Stress–inelastic strain relation for compression applied in CDP model.

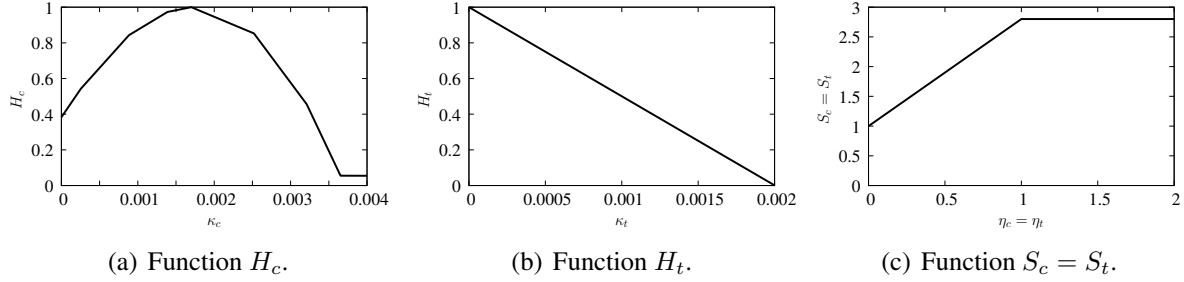


**Figure 5:** Material functions for Hoffman viscoplasticity.

### 3.2 Results for concrete damaged plasticity

The results for the CDP model are discussed at first. Fig. 6(a) shows of total force applied to the beam with the notch versus crack mouth opening displacement (CMOD). They are depicted for specimens DN1–DN4 and compared with experimental diagrams taken from [9]. It is seen that the load carrying capacity obtained for the CDP model is quite close to the experimental result, however the character of post-peak equilibrium paths is different. Numerical results give more ductile response and tending in the post-peak phase to a residual plateau rather than ceasing to zero. The CDP model exhibits a strong size effect reproducing behaviour of plain concrete specimens in experiments in a good manner. In the diagrams presented in Fig. 6(b) so-called ligament stress is calculated in the following way:

$$\sigma_{\text{lig}} = \frac{3}{2} \frac{F S}{t (D_{\text{lig}})^2} \quad (17)$$

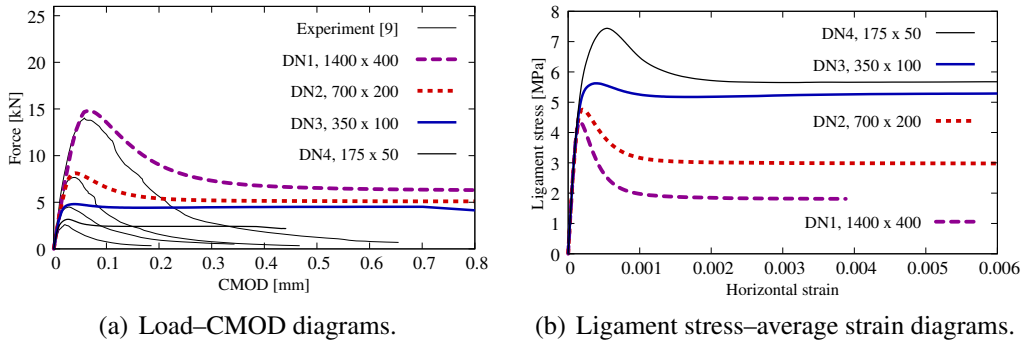


**Figure 6:** Beam with notch – diagrams for CDP model.

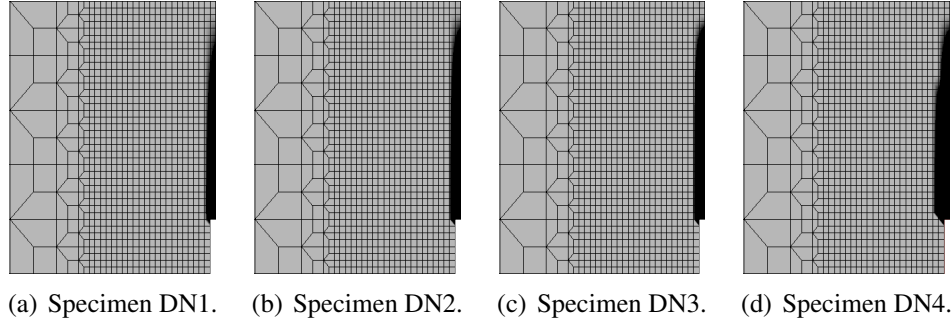


**Figure 7:** Beam with notch– distribution of equivalent tensile plastic strain (PEEQT) in final state for CDP model.

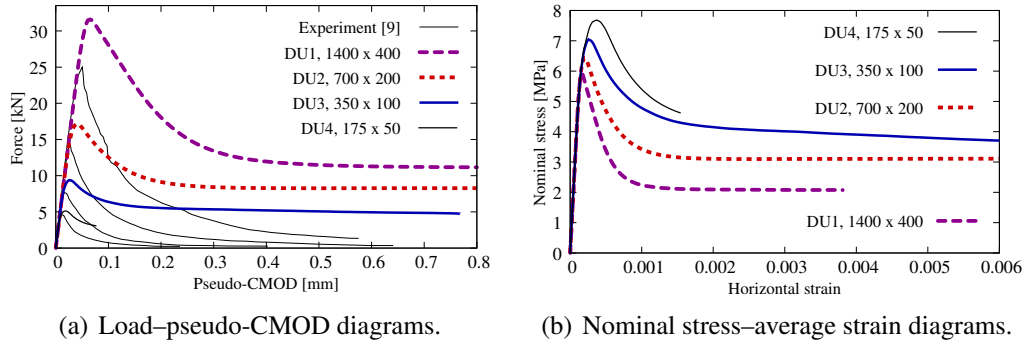


**Figure 8:** Unnotched beam – diagrams for CDP model.

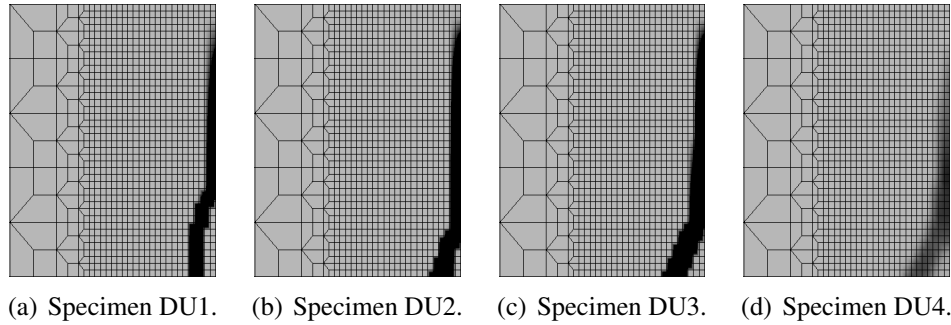


**Figure 9:** Unnotched beam – distribution of equivalent tensile plastic strain (PEEQT) in final state for CDP model.

where  $F$  is the force,  $S$  is the span,  $t$  is the thickness and  $D_{\text{lig}}$  is the ligament height in the notch region of the beam. Horizontal strain is obtained from the CMOD divided by the base  $L_m$ . Fig. 7 presents contour plots of the distribution of the equivalent tensile plastic strain (PEEQT) for four beam sizes.

Analogical results, but for the unnotched beam are depicted in Figs 8 and 9. It is observed that the load carrying capacity is overestimated in comparison to experiment [9], see Fig. 8(a). Here the so-called pseudo-CMOD is measured at the bottom surface between points  $L_m$  away from each other. In Fig. 8(b) nominal stress is derived according to Eq. (17), but now the total height  $D$  is taken into account. Again, the size effect is noticed. Fig. 9 illustrates the distribution of the equivalent tensile plastic strain (PEEQT) for all specimens DU1–DU4.

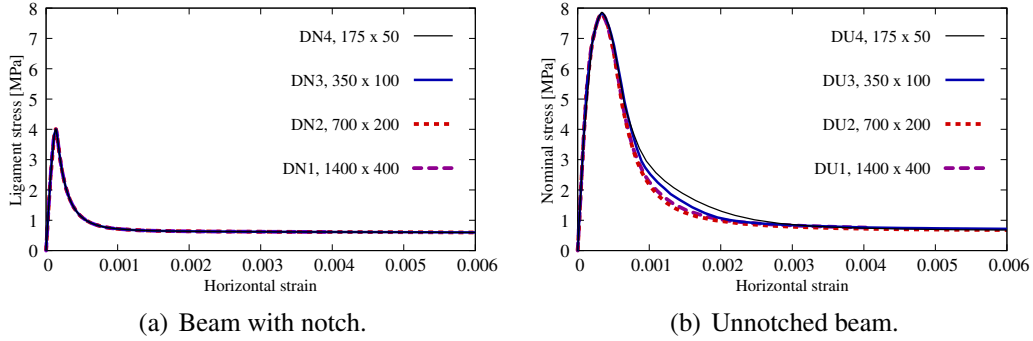


**Figure 10:** Ligament/nominal stress vs average strain diagrams for CDP model without active viscous term,  $\mu = 0$ .

The diagrams presented in Fig. 10 are prepared for the CDP model without active viscous term, i.e. the relaxation time parameter  $\mu$  equals 0. It means that in these computations local version of the model is employed and as expected the size effect does not occur.

### 3.3 Results for consistency viscoplasticity

Fig. 11 presents the diagrams for the HVP model in case of the beam with the notch. Computed post-peak equilibrium paths shown in Fig. 11(a) are much stiffer than the experimental results and very slowly tend to zero. The size effect is barely visible, see Fig. 11(b). Contour plots of the parameter  $\kappa_t$  which describes the equivalent plastic strain in tension are illustrated in Fig. 12. These crack patterns are noticeably different from those obtained for the CDP model (cf. Fig. 7) and seem to be not physically motivated. When viscous functions  $S_c = S_t$  given in Fig. 5(c) are artificially increased 3.6 times the size effect becomes more evident (Fig. 13), however still remains much smaller than that from the experiment.

The results for unnotched beams are shown in Figs 14–15. The size effect manifests itself only at the peak and just after it all curves overlap, see Fig. 14(b). In this case contour plots of the internal variable  $\kappa_t$  in Fig. 15 also differ from the results computed for the CDP model.

When the viscous term is excluded by setting  $S_c = S_t \equiv 1.0$  the size effect is absent as expected, see the diagrams in Fig. 16. However, the larger maximum stress obtained for the beam with the notch is to the contrary to the experimental evidence.

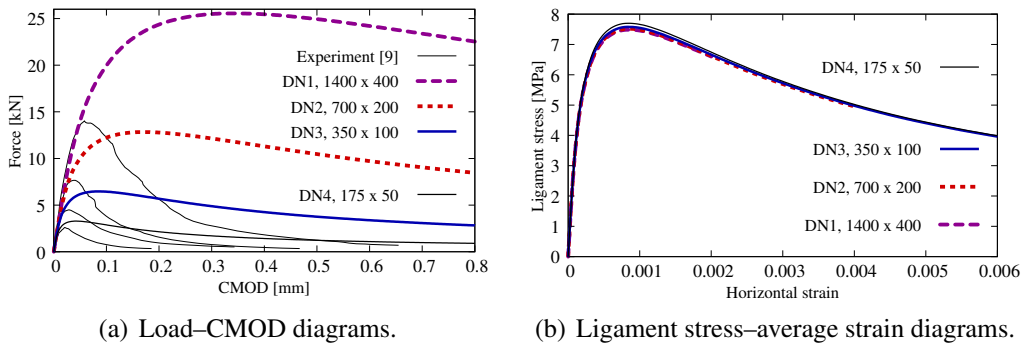


**Figure 11:** Beam with notch – diagrams for HVP model.

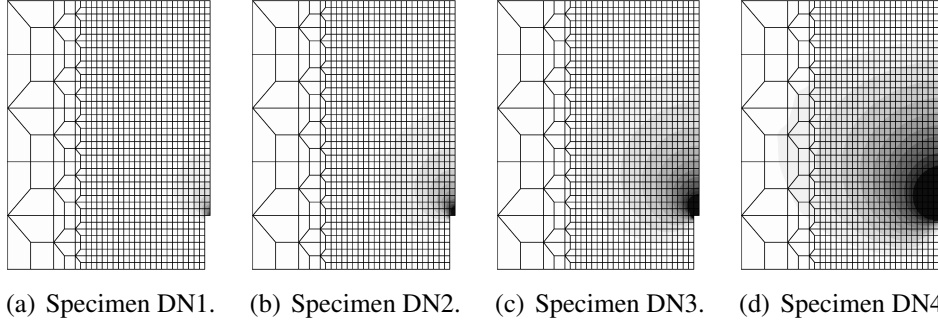


**Figure 12:** Notched beam – distribution of internal variable  $\kappa_t$  in final state for HVP model.

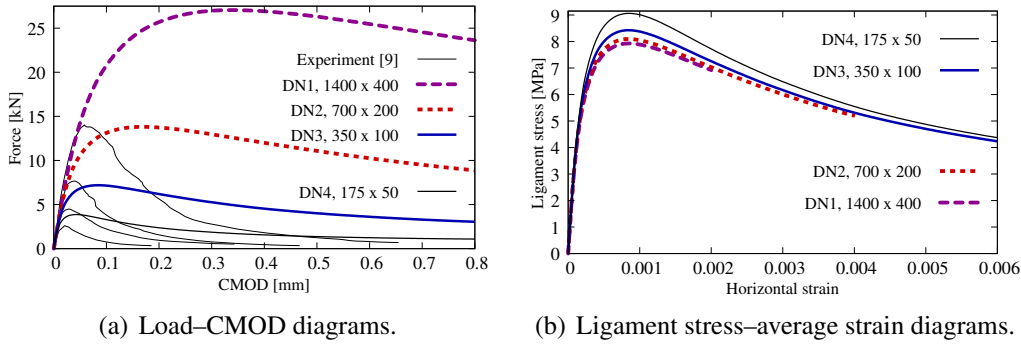


**Figure 13:** Beam with notch – diagrams for HVP model with more active viscous term.

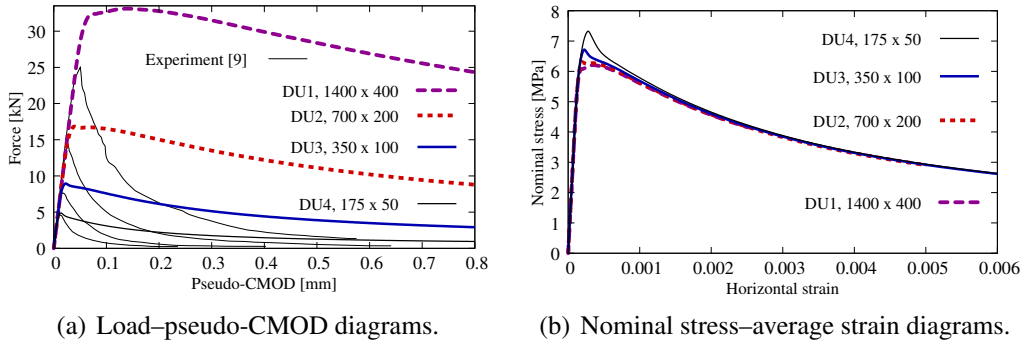


**Figure 14:** Unnotched beam – diagrams for HVP model.

## 4 CONCLUSIONS

It is well-known that non-local constitutive models are capable of reproducing the deterministic size effect due to the presence of an internal length parameter. In concrete damaged plasticity (CDP) and Hoffman viscoplastic consistency (HVP) models it is done via activation of the viscous term. In the paper these viscoplastic models are confronted on the example of the beam with and without the notch. Comparison of the size effect for both models and also experimental data [9] is depicted in Fig. 17. Logarithmic scale is used for both axes. They behave in different ways. The CDP model exhibits a pronounced size effect not only for the reached maximum strength, but also in the post-peak regime, i.e. different values of the fracture energy

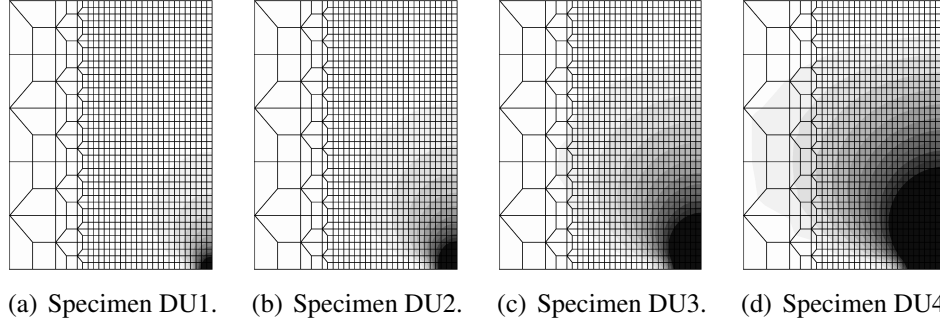


**Figure 15:** Unnotched beam – distribution of internal variable  $\kappa_t$  in final state for HVP model.

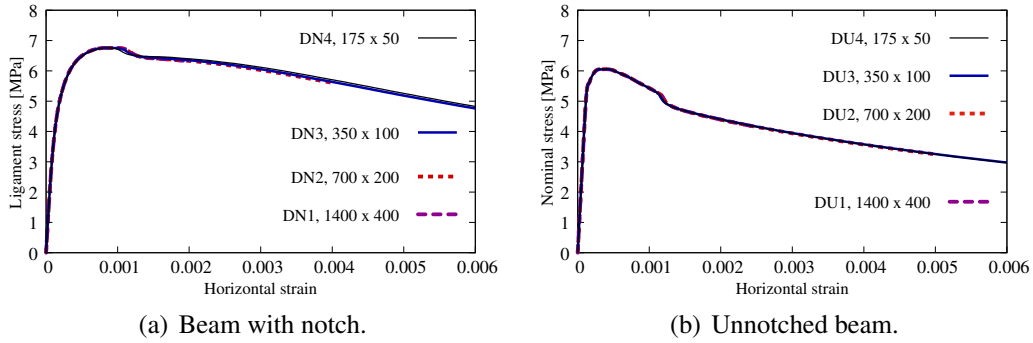


**Figure 16:** Ligament/nominal stress vs average strain diagrams for HVP model without active viscous term,  $S_c = S_t \equiv 1.0$ .

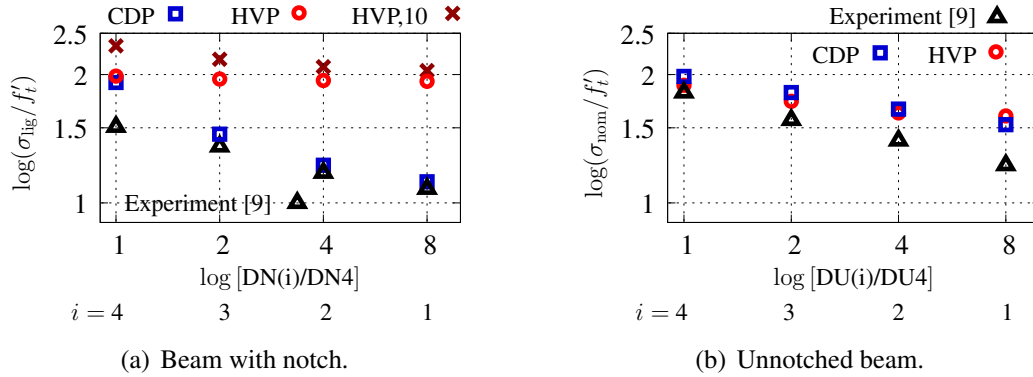


**Figure 17:** Size effect plots.

as the parameter of ductility are noticeable. The response of the HVP model is not clear in the context of the size effect. In the beam test with notch the size effect for the initial adopted data is invisible. The ability of the model in this regard is demonstrated for functions of the equivalent viscoplastic strain rate  $S_c = S_t$  with a higher limit value, i.e. when the viscous term is more active. Significant disagreement of softening zones between two considered viscoplastic models is noticed, so in the HVP model the non-associated flow rule should be introduced and further parametric studies are therefore necessary.

## REFERENCES

- [1] Z. P. Bažant and J. Planas. *Fracture and Size Effect in Concrete and Other Quasibrittle Materials*. CRC Press, 1998.
- [2] M. R. A. van Vliet. *Size effect in tensile fracture of concrete and rock*. Ph.D. dissertation, Delft University of Technology, Delft, 2000.
- [3] J. G. M. van Mier. *Concrete Fracture: A Multiscale Approach*. CRC Press, Boca Raton, 2013.
- [4] Z. P. Bažant and Q. Yu. Universal size effect law and effect of crack depth on quasi-brittle structure strength. *ASCE J. Eng. Mech.*, 135(2):78–84, 2009.
- [5] C. Le Bellégo, J. F. Dubé, G. Pijaudier-Cabot, and B. Gérard. Calibration of nonlocal damage model from size effect tests. *Eur. J. Mech. A/Solids*, 22(1):33–46, 2003.
- [6] R. de Borst and M. A. Gutiérrez. A unified framework for concrete damage and fracture models including size effects. *Int. J. Fracture*, 95(1-4):261–277, 1999.
- [7] L. J. Sluys. *Wave propagation, localization and dispersion in softening solids*. Ph.D. dissertation, Delft University of Technology, Delft, 1992.
- [8] R.L. Taylor. FEAP – A Finite Element Analysis Program, Version 7.4, User manual. University of California at Berkeley, Berkeley, 2001.
- [9] D. Grégoire, L. B. Rojas-Solano, and G. Pijaudier-Cabot. Failure and size effect for notched and unnotched concrete beams. *Int. J. Num. Anal. Meth. Geomech.*, 37(10):1434–1452, 2013.
- [10] J. Lubliner, J. Oliver, S. Oller, and E. Oñate. A plastic-damage model for concrete. *Int. J. Solids Struct.*, 25(3):299–326, 1989.
- [11] J. Lee and G.L. Fenves. Plastic-damage model for cyclic loading of concrete structures. *ASCE J. Eng. Mech.*, 124(8):892–900, 1998.
- [12] SIMULIA. Abaqus Manual (6.14). Dassault Systemes, Providence, RI, USA, 2014.
- [13] G. Duvaut and I. J. Lions. *Les Inéquations en Mécanique et en Physique*. Dunod, Paris, France, 1972.
- [14] P. Perzyna. Fundamental problems in viscoplasticity. In *Recent Advances in Applied Mechanics*, volume 9, pages 243–377, New York, USA, 1966. Academic Press.
- [15] W. Wang. *Stationary and propagative instabilities in metals - a computational point of view*. Ph.D., TU Delft, the Netherlands, 1997.
- [16] N. Bićanić, C. J. Pearce, and D. R. J. Owen. Failure predictions of concrete like materials using softening Hoffman plasticity model. In H. Mang, N. Bićanić, and R. de Borst, editors, *Computational modelling of concrete structures, Euro-C 1994*, volume 1, pages 185–198, Swansea, UK, 1994. Pineridge Press.
- [17] A. Winnicki, C. J. Pearce, and N. Bićanić. Viscoplastic Hoffman consistency model for concrete. *Comput. & Struct.*, 79:7–19, 2001.
- [18] P. A. Vermeer and R. de Borst. Non-associated plasticity for soils, concrete and rock. *Heron*, 29(3), 1984.